Journal of Colloid and Interface Science **245,** 325–337 (2002)
doi:10.1006/jcis.2001.8003, available online at http://www.idealibrary.com on IDEAL®

Analysis and Characterization of Relative Permeability and Capillary Pressure for Free Surface Flow of a Viscous Fluid across an Array of Aligned Cylindrical Fibers

Zuzana Dimitrovova*,[1] and Suresh G Advani†,[2]

*Departamento de Engenharia Mecanica, Instituto Superior Tecnico, Av. Rovisco pais, 1, 1049-001 Lisboa, Portugal; and †Department of Mechanical Engineering, Center for Composite Materials, University of Delaware, 126 Spencer Laboratory, Newark, Delaware 19716

Received April 30, 2001; accepted October 1, 2001; published online December 6, 2001

In LCM processes of fiber-reinforced composite manufacturing, resin is injected into a closed mold with a preplaced stationary fiber preform. If these preforms are created from fiber tows, resin progression at the microlevel during infiltration is often non-uniform. Consequently, macroscopic description of the filling phase requires a theory of flow through unsaturated porous media in which the transition (partly saturated) region must be taken into account. Unsaturated flows must consider surface tension effects; therefore, capillary pressure and relative permeability must be included in governing equations. This paper presents a methodology to determine relative permeability and macroscopic capillary pressure for simple flows. The results lead to important conclusions and the methodology can be generalized to other flow fields. © 2002 Elsevier Science

Key Words: **dual porous media; liquid composite molding; relative permeability; capillary pressure; surface tension; free surface flow.**

1. INTRODUCTION

In the past three decades, fiber-reinforced composite materials have become an important class of engineering materials because (i) they allow flexibility in the design of the component, (ii) of the possibility of tailoring their properties to industrial requirements, and (iii) of the development of efficient manufacturing processes.

Reinforcing fibers carry most of the structural loads; hence, more fibers translate into stiffer and stronger composite. To obtain higher fiber volume fractions, the fibers must be aligned and grouped in fiber tows (bundles) that may contain from 2000 to 48,000 fiber strands (fibrils). Fiber tows can then be arranged randomly; however, very high fiber volume fractions can only be achieved if the tows are stitched or woven to make a pattern of a fabric layer.

In polymer composites, the empty space between fibers is filled with a resin. A manufacturing process that is widely used to accomplish this task is called liquid composite molding (LCM), in which a fiber network consisting of fabric layers, called fiber preform, is placed into a closed mold and a low viscosity resin is injected into it to fill the empty spaces between the stationary fibers (1). Special attention must be paid to the injection phase as any unfilled region known as a void or a dry spot can be detrimental to the mechanical performance of the composite.

Infiltration of the resin is driven by the hydrodynamic pressure gradient originated by the inlet pressure. When the resistance of the preforms to overcome is very high, in certain regions the hydrodynamic pressure gradient can be so low that the wicking gradient can exceed it and change the driving mechanism. This situation occurs more often when dual porosity preforms (built from fiber tows) are used because the spacing between the tows is about an order of magnitude higher than the spacing of pores inside the tows. Therefore, when the inlet pressure is high, resin proceeds rapidly in intertow spaces, where the permeability is at least one to two orders of magnitude higher than in the intratow spaces. On the other hand, when the inlet pressure is low, capillary forces (higher in intratow spaces) can exceed viscous forces and the resin front will proceed more rapidly inside the tows. As a consequence resin progression is not uniform at the microlevel.

When the mold containing fibers and air is filled, air can be displaced either by a primary or by a secondary mechanism. The primary mechanism is to displace the air with the resin and allow it to escape through a vent in the mold. However, if air is trapped and held by capillary forces in the form of bubbles after the primary mechanism is completed, it can only be displaced by the secondary mechanism. To activate it, it is necessary to increase the viscous forces (e.g., by increasing the pressure) until they exceed the capillary forces.

In order to predict and consequently prevent voids and dry spot formation in flows with non-uniform progression at the microlevel, a theory of flows through unsaturated porous media must be invoked; thus, relative permeability and macroscopic capillary pressure must be included in the governing equations. This paper presents a methodology to determine the flow

[1] E-mail: zdimitro@dem.ist.utl.pt.

[2] To whom correspondence should be addressed. Fax: (302)831-3619. E-mail: advani@me.udel.edu.

0021-9797/02 $35.00

characteristics for simple flows. The results lead to important conclusions and the methodology can be generalized to other flow situations.

2. MACRO LEVEL GOVERNING EQUATIONS

Practice has converged on modeling of filling as flow through a porous medium, which is created by the fiber network (2–7). Basic literature on flow through porous media is covered in books such as (8–10). Attention was focused on the macrolevel (global) analysis, which is assumed as a *quasi-steady-state process* and the domain to be filled was divided into two regions, saturated and unfilled, separated by a *moving sharp surface* representing the flow front. Thus, only the theory of saturated flows was required for description of the filling process. Such an approach describes solely the primary displacing mechanism and we will refer it as the *standard approach*. There are only few works related to the secondary mechanism (11, 12) and little attention has been paid to unsaturated flows in dual scale porous media.

Under assumptions reasonable for most LCM processes, i.e., for isothermal quasi-steady filling of incompressible and stationary preform by an incompressible Newtonian resin with insignificant resin inertia as compared to viscous effects, with no influence of resin weight and of the air on the resin front, one can write the governing equations for the standard approach as follows,

$$\nabla \cdot \mathbf{v}^{\mathrm{D}} = 0, \qquad [1a]$$

$$\mathbf{v}^{\mathrm{D}} = -\frac{\mathbf{K}}{\mu} \cdot \nabla P \qquad [1b]$$

with the following boundary conditions,

$$\text{at the resin front, } \partial f/\partial t + (\mathbf{v}^{\mathrm{D}} \cdot \nabla f)/\phi = 0 \qquad [2a]$$

$$\text{and} \quad P = 0; \qquad [2b]$$

$$\text{at the mold walls, } \mathbf{v}^{\mathrm{D}} \cdot \mathbf{n} = v_{\mathrm{n}}^{\mathrm{D}} = 0 \Rightarrow K_{\mathrm{nn}} \frac{\partial P}{\partial n} + K_{\mathrm{nl}} \frac{\partial P}{\partial l} = 0; \qquad [2c]$$

$$\text{at the injection gates, } \mathbf{v}^{\mathrm{D}} = \mathbf{v}_0(t) \quad \text{or} \quad P = P_0(t); \qquad [2d]$$

where $\mathbf{v}^{\mathrm{D}}$ is the phase-averaged velocity vector related to the intrinsic phase average $\mathbf{v}^{\mathrm{f}}$ by $\mathbf{v}^{\mathrm{D}} = \phi \mathbf{v}^{\mathrm{f}}$, ϕ being the porosity, and P is the intrinsic phase-averaged pressure (pore pressure). $\mathbf{K}$ is the permeability tensor of the fiber preform and μ is the resin viscosity. Implicit function $f(\mathbf{x}(t), t) = 0$ describes the location of the moving resin front. Equation [2a] results from conservation of mass, it is the motion equation of the front, and it is known as the kinematic equation, while Eq. [2b] is the static (sometimes dynamic) free boundary condition. t, $\mathbf{n}$, $\mathbf{v}_0$, or P_0 stand for time, outer unit normal to the front, and prescribed velocity and pressure at the inlet, respectively.

P and $\mathbf{v}^{\mathrm{D}}$ are used as the macroscopic (global) counterparts of the microscopic (local) pressure p and velocity vector $\mathbf{v} \cdot \mathbf{K}$ may be determined by analytical (13–16), experimental (7, 17–26) or numerical methods (10, 27–31). Numerical or analytical determination of $\mathbf{K}$ is conducted by microlevel analysis. This is accomplished by calculating the phase average of the local velocities of the unit viscosity Stokes flow in a fully saturated basic cell or a representative volume element under a unit macropressure gradient or a unit volumetric force. For basic unit cell, periodic boundary conditions are applied.

However, Eq. [1] originally was an empirical relation proposed by Darcy (32). It has been verified analytically by homogenization techniques, namely by asymptotic expansion methods (27, 33–34) and by local averaging methods (10, 35).

Numerical-simulation results from standard approach for single scale porous preforms or for dual scale porous preforms with randomly arranged fiber tows usually showed excellent agreement with experimental examinations. However, in woven or stitched dual porous preforms, macroscopic flow front is not sharp and a *transition layer of finite depth* between the saturated and unfilled region is visible. This occurs as a consequence of the non-uniform progression at the microlevel, as noted in the introduction. In order to describe the transition region it is necessary to modify Eq. [1] to

$$\phi \frac{\partial s}{\partial t} = -\nabla \cdot \mathbf{v}^{\mathrm{D}}(s), \qquad [3a]$$

$$\phi s \mathbf{v}^{\mathrm{f}}(s) = \mathbf{v}^{\mathrm{D}}(s) = -\frac{k(s)}{\mu} \mathbf{K} \cdot \nabla (P(s) - P_{\mathrm{c}}(s)), \qquad [3b]$$

where the new variable, saturation s, is defined as the ratio of the filled pore space to the total pore space in a basic unit cell or a representative volume element. In the transition region s belongs to the open interval (0,1) and in the saturated region (when $s = 1$) Eq. [3] coincides with Eq. [1]. Because exact implementation of Eq. [3a] is quite difficult (36), usually an extension of Darcy's law in the form of Eq. [3b] (first proposed by Muskat in (37)) is used. $k(s)$ is referred to as the relative permeability and takes values in the closed interval [0,1]; for the sake of nonambiguity, the term absolute permeability is used for $\mathbf{K}$. In the same way as single porosity absolute permeability **K,** dual porosity $\mathbf{K}$ can be determined from fully saturated flow in a basic cell or a representative volume element, either with all single fibrils modeled (38, 39) or with fiber tows approximated by a porous medium (30, 40, 41). Unlike saturated flows, unsaturated flows must consider capillary effects; therefore, besides the global hydrodynamic pressure $P(s)$ the macroscopic capillary pressure $P_{\mathrm{c}}(s)$ appears in [3b]. One needs to find $P(s)$ but $P_{\mathrm{c}}(s)$ and $k(s)$ enter the analysis as known functions; thus, they must be determined either experimentally or by transient microanalysis.

Applicable boundary conditions are only Eqs. [2c] and [2d] and will remain unchanged. Resin progression is ensured by saturation increase, i.e., by Eq. [3a], and actually the term "resin front" cannot be used anymore. The macroscopic capillary pressure, unlike its microscopic counterpart, does not act at the resin front, but in the full transition region. It can be proved, as by

Antonelli and Farina (42), that if the depth of the transition region tends to zero, then the approach based on Eq. [3] tends to the standard approach. The explicit or implicit method can be easily implemented in Eq. [3a], but unlike the advantage of the explicit method in standard approach, stable results can only be obtained by use of central differences and implicit methods when the capillary pressure dominates (43).

It is useful to introduce one more level, which we will refer to as the *mesolevel*, as an intermediate level between the macro- and microlevel (38). Then the macrolevel maintains the full medium scale. Microlevel will be reserved for intratow scale and intertow scale will correspond to the mesoscale. At the mesoscale, resin motion in the intertow spaces is described by the Stokes flow while the fiber tows can model as the porous medium with the corresponding Darcy law. Transient mesoanalysis can be then used to determine $k(s)$ or $P_c(s)$. However, the main purpose of the mesoscale analysis should be to capture void formation and to study other particular details of the flow progression, which cannot be modeled by macro- or microanalysis.

3. MICROLEVEL GOVERNING EQUATIONS

Description of the transition region must originate at the microlevel. With the assumptions stated at the beginning of the previous section, one changes the law from Darcy's law to Stokes law to obtain the governing equations. The filled region is separated from the rest by a sharp flow front with "material discontinuity"; thus, the explicit method for the front progression becomes advantageous. Governing equations in the resin domain are

$$\nabla \cdot \mathbf{v} = 0, \qquad [4a]$$

$$\nabla p = \mu \Delta \mathbf{v}, \qquad [4b]$$

where $\mathbf{v}$ and p denote the local velocity and pressure, respectively, and μ is the resin viscosity. Boundary conditions are usually written as (44) follows:

$$\text{at the resin front, } \partial f/\partial t + \mathbf{v} \cdot \nabla f = 0 \quad \text{and} \qquad [5a]$$

$$\boldsymbol{\tau}^{v} \cdot \mathbf{n} = \mathbf{0} \text{ and } p = p_c = -\gamma\left(\frac{1}{R_1} + \frac{1}{R_2}\right) = -2\gamma H; \qquad [5b]$$

$$\text{at the fiber boundary, } \mathbf{v} = \mathbf{0}; \qquad [5c]$$

$$\text{at the inlet, } \mathbf{v} = \mathbf{v}_0(t) \quad \text{or} \quad p = p_0(t). \qquad [5d]$$

Function $f(\mathbf{y}(t), t) = 0$ again describes the position of the moving front (spatial variable at the microlevel is usually rescaled and designated as $\mathbf{y}$), $\mathbf{n}$ is the outer unit normal vector to the corresponding surface, $\boldsymbol{\sigma}$ is resin stress tensor, and $\boldsymbol{\tau}^{v}$ is viscous shear stress. R_1 and R_2 are the radii of the surface curvature, H is the mean curvature, and γ is the surface tension coefficient. Equation [5b] expresses the surface tension influence, which at a curved resin front surface at equilibrium can be replaced by a pressure drop Δp called the capillary pressure, p_c (45). The relation does not determine the actual equilibrium free surface shape, it only tells us what distribution of the capillary pressure should be applied at the known frontal surface. In Eq. [5b], as usual, viscous normal stresses were neglected as compared to pressure values.

Besides the fact that Eqs. [5a]–[5d] must be fulfilled, a contact angle, θ, must be formed at the resin surface-fiber contact point. Actually, then the no-slip condition Eq. [5c] is quite inappropriate and slip coefficients are usually used to remove the stress singularity there (47). The contact angle is given by Young's equation, presented in (8, 10, 44–46), but the equation itself is not important for our purposes. Surface tension and contact angle are definite and accurately measurable properties; thus, they will be introduced into our studies as known parameters. It is useful to remark that the resin front shape is formed in a way that equilibrium is reached between all unbalanced forces. If only surface tension effects are considered and all other contributions are neglected, then surface with constant curvature is formed (48).

Before we proceed, is it important to review some facts and introduce new terms. The term, *basic cell*, ϑ, is used in *asymptotic expansion methods* as the smallest component of a periodic medium, which can form the full medium by its periodic repetition. An infinite number of different basic cells exists in one periodic medium, but homogenization results cannot depend on its choice. We will introduce the term *periodic solution* for the solution ($\mathbf{v}$, p) of Stokes problem in a fully saturated basic cell under periodicity boundary conditions, i.e., of the problem stated by Eqs. [4] and [5c] and by the following conditions,

$$G \cdot \xi \text{ is prescribed on all external cell boundaries} \quad \text{and} \qquad [6a]$$

$$\mathbf{v} \text{ and } \tilde{p} \text{ fulfill periodicity boundary conditions on all external cell boundaries.} \qquad [6b]$$

$G < 0$ is an imposed macrogradient, ξ is a spatial coordinate inside the basic cell, and $\tilde{p}$ is defined by $p = G \cdot \xi + \tilde{p} + c$; $\mathbf{v}$ is unique and p is unique up to a constant pressure field c. $G \cdot \xi + c$ is called the linear, while $\tilde{p}$ is called the periodic part of the local pressure. Viscosity enters the problem only as a linear analysis parameter; surface tension and contact angle do not appear at all. Usually it is not necessary to prescribe $G \cdot \xi$ on all external boundaries, e.g., when the basic cell has one boundary as inlet and some other as outlet, and then it is possible to prescribe $G \cdot \xi$ only there. Volume rate at the outlet is naturally the same as at the inlet, but velocity distribution along the outlet boundary will generally be different. Exploiting incompressibility and the no-slip condition, the ith component of phase-averaged velocity can be determined by (31)

$$|\vartheta| v_i^D = \int_{\vartheta_r} v_i \, d\mathbf{y} = \int_{\vartheta_r} v_k \frac{\partial y_i}{\partial y_k} \, d\mathbf{y} = -\int_{\vartheta_r} \frac{\partial v_k}{\partial y_k} y_i \, d\mathbf{y} + \int_{s_{rf}} v_k n_k y_i \, d\mathbf{S} + \int_{\partial\vartheta_e} v_k n_k y_i \, d\mathbf{S} = \int_{\partial\vartheta_e} v_k n_k y_i \, d\mathbf{S}, \qquad [7]$$

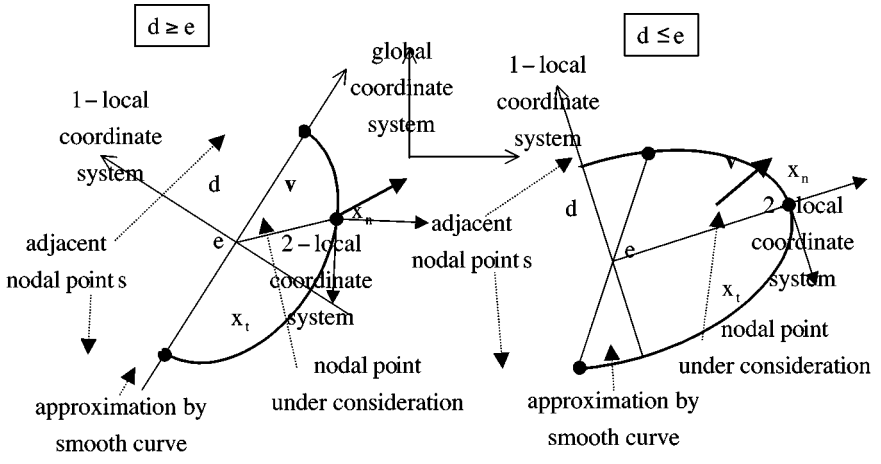

FIG. 1. Two ways to approximate the flow front with a smooth curve and specify the 2nd coordinate system.

where ϑ_r is the part of the basic cell occupied by the resin, S_{rf} is the resin-fiber boundary, and $\partial\vartheta_e$ is the external cell boundary. Thus, if along the inlet and outlet boundary velocity distributions do not coincide and y_i is not constant, then the averaged value cannot correspond to the averaged periodic velocity.

4. FREE BOUNDARY PROGRAM

With the purpose of examination of the resin flow at the microlevel and of determination of relative permeability and macroscopic capillary pressure, a free boundary program using the general purpose finite element code Ansys (exploiting the Ansys Parametric Design Language (APDL)) was developed, so far only for 2D problems. Its initial form without surface tension influence was presented in (39). The program permits one to run transient microlevel problems under the assumptions listed in the previous section. A new resin front position is calculated directly using the free boundary condition Eq. [5a] and explicit methods.

At an arbitrary frontal nodal point at current time, t_k, a one time step run follows as first, velocity is extracted from previously solved Stokes problem at this nodal point and a local coordinate system (called 1-local coordinate system as shown in Fig. 1) is created close to it, where the flow front is locally approximated by a smooth curve including two adjacent nodal points. This permits one to define uniquely the outer normal vector to the flow front. Two different ways to approximate are explained in Fig. 1. An elliptic approximation in lieu of a circular or a parabolic one was found preferable. Next, a second local coordinate system is created at the nodal point under consideration with axes along the tangential, x_t, and the outer normal vector, x_n. If the flow front is described locally by $x_n = g(x_t)$ with respect to the second coordinate system, then Eq. [5a] can be written as

$$v_n - v_t \frac{\partial g}{\partial x_t} = v_n = \frac{\partial g}{\partial t}. \qquad [8a]$$

In explicit scheme, the new nodal position is determined in the normal direction as

$$x_{n,t_{k+1}} = x_{n,t_k} + (t_{k+1} - t_k) v_{n,t_k}. \qquad [8b]$$

The smooth curve approximation as described above is repeated now for the new front, and the surface curvature and consequently capillary pressure according to Eq. [5b] are calculated separately at each new frontal nodal point. Capillary pressure is then imposed as piecewise linear at each frontal element edge. Other boundary conditions Eqs. [5c–5d] are applied and, finally, Stokes problem is solved in the new domain.

Treatment of nodal points at axes of symmetry is adjusted to their special location and also resin surface-fiber contact points are handled differently. If surface tension effects are neglected, then resin front progresses along the fiber boundary when other frontal points will touch it, as it is shown in Fig. 2a. If surface tension effects are included, the contact angle is adjusted to its given value by creating an additional curved surface as shown in Fig. 2b. The radius of this surface is not a known priority, but it should be small, in order not to affect the progression of the bulk boundary. In accordance with the real resin

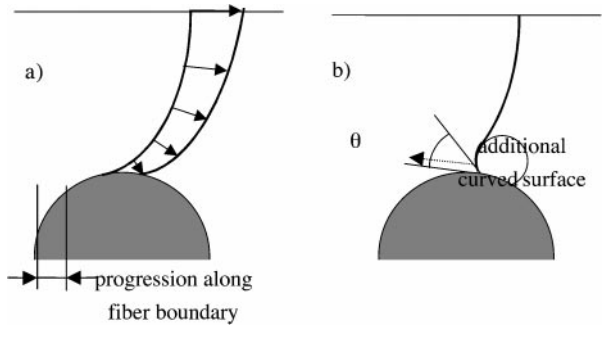

FIG. 2. Progression of the resin front along the fiber boundary, without (a) and with (b) surface tension effects included.

behavior, it is ensured in the program that once a fiber surface is wetted, it remains wetted. This does not hold generally for the bulk flow front; spaces filled by the resin can be abandoned later, as will be seen in examples in the next section. Adjustment of the resin front to the contact angle is very important, in order to ensure the correct total value of the capillary pressure applied at the frontal surface. It can be proved that capillary pressure acting on an arbitrary part of a free surface satisfies equivalent load conditions with the surface tension applied in the cuts of this surface. Thus, the total capillary pressure, i.e., the capillary force, which should be applied at the resin front, can always be determined analytically if the resin front-fiber contact point locations (and the parameters γ and θ) are known.

Several adjustments of the frontal nodal points are implemented in the free boundary program during one time step run. First, very close nodal points are eliminated at the old front, in order not to affect the approximation of a smooth curve. The new front extent is always reduced not only by the frontal ratio, but it is also reduced in the way that the boundary will not cross any of the other boundaries (symmetry or fiber), but at best will touch them. Other reduction eliminates crossing of normals during front determination and loops creation along the front. Again, very close nodal points of the new front are eliminated.

An implicit method is also implemented into front progression in which way $v_{n,t_{k+\alpha}}$ are used in Eq. [8b] with $\alpha \in (0, 1]$. Iterations are performed over different domains, yielding slow convergence properties; thus, it is not worthwhile to use it. Accuracy of the new front position can be gained in the explicit approach by measured time steps. In the program, time step is calculated from the maximum allowed frontal extent, which is defined as a ratio of the maximum finite element size of frontal elements. This ratio, which we call as the *frontal ratio*, as well as the element size are user-input parameters. The program allows one to restart at the user-specified time step and modify the parameters for the subsequent analysis. A criterion when to decrease the frontal ratio does not have to be determined analytically. The best warning that the frontal ratio is too high is when the new front is not smooth. This can happen basically due to two reasons, either there will be a large change in the normal velocity or if the capillary number of the problem is very low, which makes the flow front numerically very sensitive to the approximation of the capillary pressure. Capillary number is a dimensionless measure of the importance of viscous over capillary forces and it is defined as the ratio of viscous forces per unit length to surface tension, as

$$N_c = \frac{v\mu}{\gamma}, \qquad [9]$$

where v is a selected characteristic velocity. When capillary number is very low, then small incorrectness caused by numerical approximations can amplify capillary pressure, which with too high frontal ratio will cause opposite curvature in consequent front. Repetition of this fact causes oscillations. The frontal ratio can naturally become so small that the front progression will practically stop. In this case the implicit scheme could help.

The free boundary program is based on a moving mesh scheme. Therefore, the flow front can be traced precisely, which is important for the application of surface tension effects. Also other advantages such as easy prescription of variable element size permiting creation of fine discretization close to the flow front and rougher discretization in other regions can be applied. Moreover, Ansys meshing capabilities can be exploited and the time taken by the mesh creation and by the solution of the (linear) analysis is almost negligible when compared to the time needed for the extraction of the velocities, the new front creation, and assessment of the results. Several Fortran files were implemented into a general APDL file with the intent of making this part of the program numerically more efficient.

5. FLOW ACROSS CYLINDRICAL FIBERS

Before the methodology for determination of the relative permeability and the macroscopic capillary pressure is presented, a simple case of flow across cylindrical fibers with circular cross section and square arrangement is discussed. Flow front variation and the time it takes to become periodic with respect to the input parameters are investigated. Fiber radius for this study was selected to be 0.25 mm and spacing of fiber centers is 1 mm (porosity is approximately 0.8), to be able to see front variations more easily.

Let the input parameters for silicon oil and carbon fibers be $\mu = 0.057\,\text{Pa} \cdot s$, $\gamma = 20.64 \times 10^{-3}$ N/m, and $\theta = 28.36^0$. The specimen chosen for the study contain five fibers and only the upper half will be examined because of symmetry. The inlet velocity is applied uniformly along the left side of the specimen and symmetry conditions are imposed on the lower and upper pore boundaries. Thus the problem is macroscopically one-dimensional or can be assumed as three-dimensional with no influence on other two directions. Five cases are examined. They correspond to $v = 1$ m/s with no influence of the surface tension and $v = 1$, 0.1, 0.01, and 0.001 m/s, respectively. These five cases yield capillary number variations as ∞, 2.76, 0.276, 0.0276, and 0.00276, respectively. Flow front progression is reported in Fig. 3; consequent fronts have the same ordering number increase, but do not correspond to the same time increase, as sometimes front ratio was changed or front extend was reduced due to other reasons. It can be concluded that different flow patterns are strongly related to the capillary number and that fronts become periodic very soon, right after the first fiber was covered with resin.

Figure 3 demonstrates that as the capillary number decreases, capillarity becomes stronger and the resin front progression pattern might approach the constant curvature pattern directed only by the contact angle, as sketched in Fig. 4. In the first case (Fig. 3a) after the top of the fiber has been passed, hydrodynamic pressure moves the resin to the next fiber and only after the resin reaches it, space between fibers begins to be filled. Without surface tension, any combination of viscosity and inlet

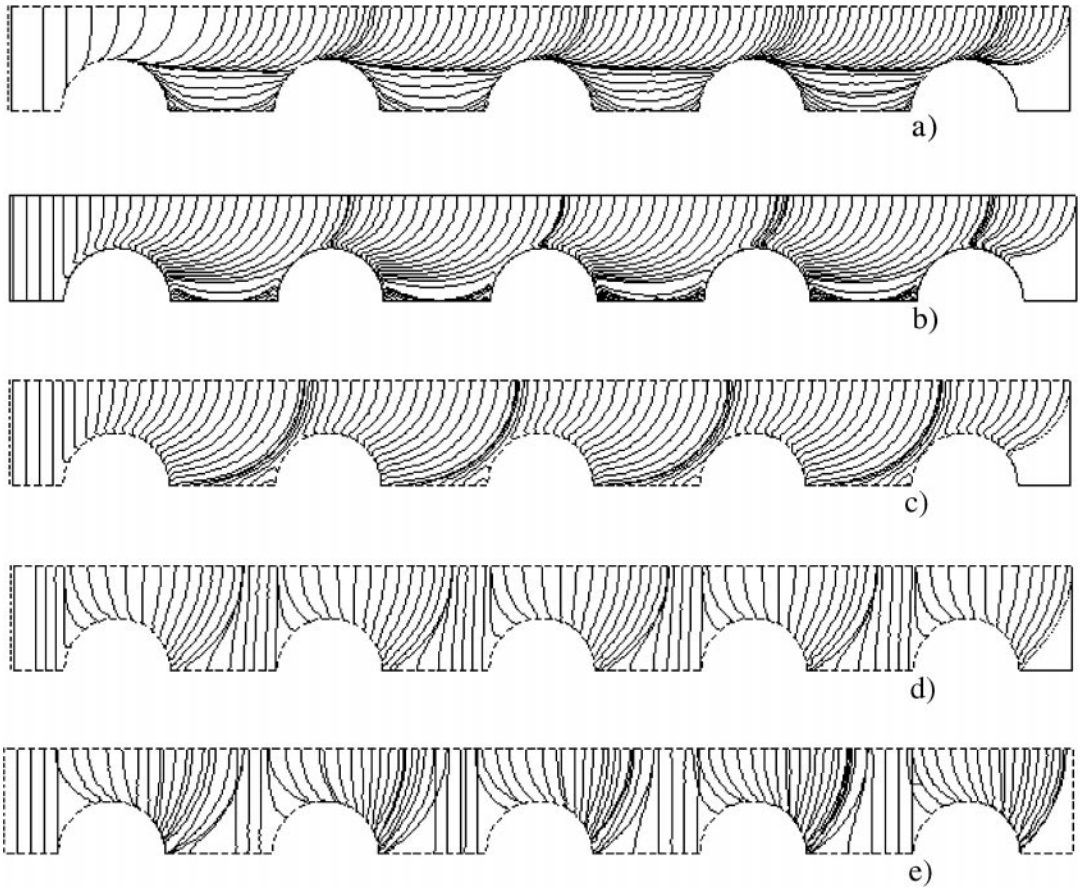

FIG. 3. Flow front variation for capillary number a) ∞, b) 2.76, c) 0.276, d) 0.0276, and e) 0.00276.

velocity yields the same front progression. In the other two cases (Figs. 3b and 3c) flow front also reaches the next fiber before the space between the fibers is fully filled. Therefore a void might be formed and our results correspond to the vacuumed initial stage. In last case (Fig. 3e), when the front reaches the fiber, the upper part moves back to adjust the "almost" constant curvature shape determined by the contact angle. But the flow front shape cannot "hold" this position because the fibers are too far and the contact angle is too high. Constant curvature surface progression directed by the contact angle (Fig. 4) is not developed. Differences between Fig. 3e and Fig. 4 are clear after the front crosses the top of the fiber. Then, influence of the hydrodynamic pressure is noticeable in Fig. 3e. The upper part of the front advances so much that after the fiber has been completely surrounded by the resin, the upper part moves back, and the resin front becomes straight. On the other hand, it is seen in Fig. 4 that without any hydrodynamic pressure, resin progression would completely stop before the last plotted positions would be reached (49).

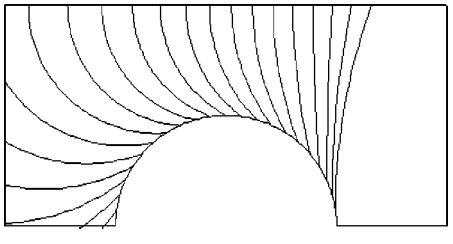

FIG. 4. Constant curvature surface progression directed solely by the contact angle.

Figures 3a and Fig. 4 correspond to two limiting cases, to progression where capillarity is neglected and to the one where only capillarity is dominant. Besides the geometry, progression in Fig. 4 is influenced by the contact angle. Thus front pattern related to this specimen under any capillary number but with contact angle maintained should be addressed between these two cases.

It was numerically justified that the front progression is the same for the same capillary number and independent of absolute dimensions (contact angle is maintained during this comparison). Flow progression for three situations with the same capillary number of $N_c = 0.276$ obtained by the following combination of parameters, (i) $\mu = 0.0057\,\text{Pa}\cdot\text{s}$, $\gamma = 20.64 \times 10^{-3}\,\text{N/m}$, and $v = 1$ m/s; (ii) $\mu = 0.057\,\text{Pa}\cdot\text{s}$, $\gamma = 206.4 \times 10^{-3}$ N/m, and $v = 1$ m/s; (iii) the case related to Fig. 3c with dimensions 10 times amplified; are presented in Fig. 5. Progressions should

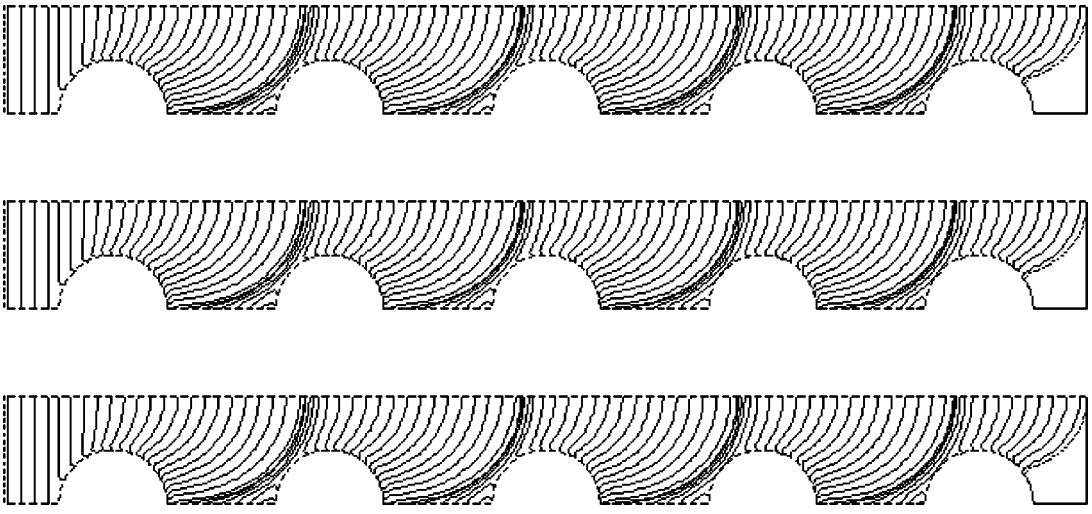

FIG. 5. Identical flow front progression for three cases of the capillary number of 0.276. This capillary number was obtained by I) modifying viscosity and velocity, II) modifying surface tension and velocity, and III) changing dimensions by rescaling.

be compared to Fig. 3c. The fact that this expected equivalence is shown numerically also verifies correctness of the free boundary program.

In summary, it was seen that flow front progression is strongly dependent on capillary number. However, once all pores are filled, local velocity and pressure in any basic cell correspond to the periodic solution, and consequently, capillarity cannot influence the absolute (saturated) permeability. In Fig. 6 the distribution of the horizontal velocity component related to progression from Fig. 3b is plotted; it is seen that it is periodic in the full part of the specimen, where flow fronts display the periodic pattern, except in the vicinity of the flow front.

For macroscopically one-dimensional (or three-dimensional with no influence on other two directions) problem we introduce the *uniform basic cell* as a basic cell, in which during resin infiltration saturation increases from 0 to 1, while previous cells are fully saturated and next cells are fully empty. Uniform basic cells depend on capillary number, because their left (inlet) and right (outlet) sides are formed by periodically corresponding flow fronts. In transition stage they are called as *transition cells*. After a transition cell is filled, it will still take additional time until the distribution of **v** and p inside it will correspond to the periodic solution (they will reach it simultaneously as a consequence of the uniqueness of the periodic solution). Based on this fact, from a theoretical point of view, the transition region should not cover only $s \in (0,1)$ but should include a part of the saturated region ($s = 1$), where local fields are not yet periodic; i.e., they do not correspond to the steady-state situation. We will refer constant flow rate filling as *uniform filling*. If any possible transition cell is filled, **v** and p resemble periodic solution if phase-averaged velocity is a linear function of ξ_s and macropressure gradient is constant and independent of the uniform cell choice. ξ_s is a spatial variable corresponding to the resin front position in cells, ranging from zero to the cell length L. Macropressure gradient is represented by the gradient of the intrinsic phase-averaged pressure with respect to ξ_s. Then it yields from Eq. [3b] that relative permeability is a linear function of ξ_s.

6. METHODOLOGY TO DETERMINE RELATIVE PERMEABILITY AND MACROSCOPIC CAPILLARY PRESSURE

Unlike absolute permeability, no simple relation is available to determine the relative permeability either from the asymptotic expansion or from the local averaging methods. A general introduction of the relative permeability notion by the local averaging method can be found in (10, 35), but it cannot be easily implemented in particular cases. Relative permeability concept is discussed in (8). Other theoretical studies, which can be found in the literature, usually deal only with particular cases, as, e.g., in

FIG. 6. Distribution of the horizontal component of the local velocity in m/s for capillary number of 0.276.

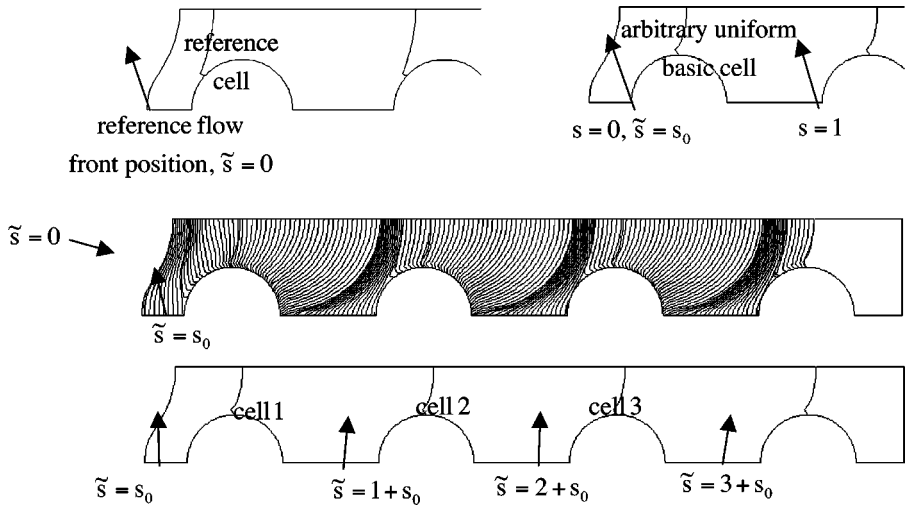

FIG. 7. Reference flow front position and the reference cell, arbitrary uniform basic cell, and flow front progression along the selected geometry.

(50). Regarding composite processing, very little experimental data are available (36, 51).

Macroscopic capillary pressure should correspond to the average of its microscopic values while resin is filling the basic cell or the representative volume element (10); thus,

$$P_c(s) = 2\gamma \langle H \rangle (s), \qquad [10]$$

where $\langle H \rangle (s)$ is the average of the mean curvature. There is no general methodology to use Eq. [10] and one cannot ensure that in periodic media such result is independent of the cell geometry. Several methodologies to represent macroscopic capillary pressure have been developed in [8–10], [51–53].

For both relative permeability and macroscopic capillary pressure, the theoretical and numerical background for LCM processes is not yet established. In this section, a methodology to determine these characteristics will be presented for a simple flow example. It will be shown that from this simple case, important conclusions can be drawn and that generalizations of the methodology are possible.

Let the geometry from the previous section be examined for flow with $N_c = 0.166$. The *principal assumption* in this analysis is that after any arbitrary transition cell is filled, local fields **v** and p will resemble *immediately the periodic solution*. If this is fulfilled, then the phase-averaged velocity in filled cells and the intrinsic phase-averaged pressure difference between neighboring filled cells would be constant and equal to the periodic value, for any choice of the uniform cell. It was verified numerically for some particular choices that the error introduced in the study due to this assumption is small.

We introduce reference saturation, $\tilde{s}$, and mark a reference flow front position where $\tilde{s} = 0$ and the corresponding uniform cell we name as the reference cell (Fig. 7). The left side of any arbitrary uniform basic cell is located in the reference cell at $\tilde{s} = s_0$. In order to compare behavior of the averaged characteristics in neighboring cells, $\tilde{s}$ is measured along the cells. Thus $\tilde{s} = n + s + s_0$, and $\tilde{s}$ higher then unity does not mean overfilling. s_0 is restricted to [0,1], $s \in [0,1]$ is reserved to mark actual flow front in the transition cell related to a particular uniform cell, and n denotes number of fully filled cells behind this transition cell (Fig. 7).

Evolution of phase-averaged velocity and intrinsic phase-averaged pressure can be expressed as functions of n, G, s, and s_0, where $G < 0$ is the macroscopic saturated (periodic) gradient. In order to provide the macroscopic pressure gradient estimation, it is convenient to switch from variables s and s_0 to spatial variables ξ_s and ξ_{s_0}, related to the filled area and defined as sketched in Fig. 8. We remark that ξ_s and ξ_{s_0} are assumed as dimensional, both ranging from 0 to $L = 1$ mm. Then the macroscopic pressure gradient in the transition cell can be estimated according to Fig. 9. At this point it is still impossible to use Eq. [3b], since then the relative permeability would depend on the uniform cell geometry. It is necessary first to average separately the phase-averaged velocity and the macroscopic pressure gradient over ξ_{s_0}. This operation will be designated as $\langle\,\rangle_{\xi_{s_0}}$. Macroscopic capillary pressure is obtained as an intermediate

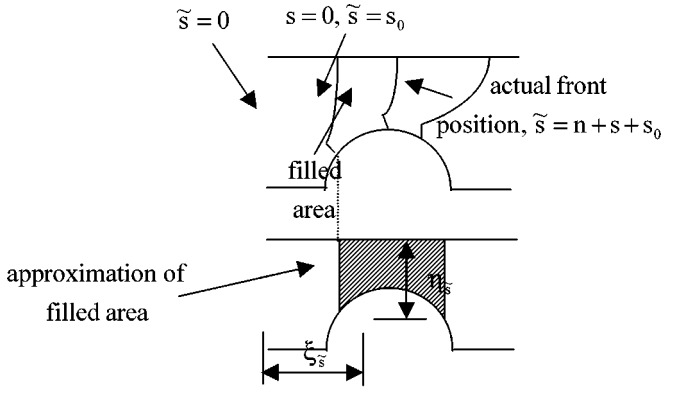

FIG. 8. Estimation of the distance $\xi_s = \xi_{\tilde{s}} - \xi_{s_0} - nL$ according to filled area (saturation).

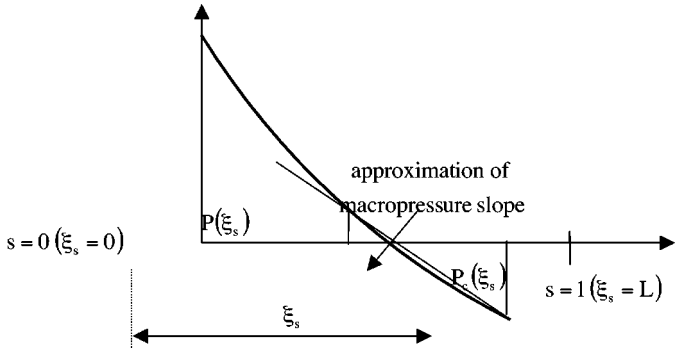

FIG. 9. Macro pressure gradient estimation in the transition cell.

result. Generalizations of this methodology will be discussed later.

In order to determine functional dependencies, an arbitrary uniform cell specified in Fig. 7 is considered. The averages are calculated at each time step in the free boundary program, separately at each uniform cell and plotted in Figs. 10 and 11. It is seen from Fig. 10 that the phase-averaged velocity (horizontal component) in transition cell is monotonically increasing and reaches the periodic value almost immediately after the transition cell is saturated. Periodic values are then maintained in the fully filled cells. Intrinsic phase-averaged pressure inside filled cells vary with saturation of their neighbors, as shown in Fig. 11.

The following derivation is fully analytical except for one particular point where we will need numerical values. Nevertheless, the form of functions introduced below was first guessed from numerical results. Let us start with macroscopic pressure gradient derivation. For intrinsic phase-averaged pressure expression in filled j cell, $P_j^{ff}(\xi_s, \xi_{s_0})$, we will use two facts: (i) it is an extension of the form for uniform filling without capillary pressure, which is simply,

$$P_j^{fu}(\xi_s, \xi_{s_0}) = -G \cdot \xi_s - G \cdot L(n - j + 1/2), \qquad [11]$$

(ii) it preserves the statement that values of local pressure between two filled neighboring uniform cells differ by GL in any case of filling, giving for a fixed front and that $\xi_{s_{02}} > \xi_{s_{01}}$

$$P_j^{ff}(\xi_s, \xi_{s_{01}}) - P_j^{ff}(\xi_s - (\xi_{s_{02}} - \xi_{s_{01}}), \xi_{s_{02}}) = -G \cdot (\xi_{s_{02}} - \xi_{s_{01}}). \qquad [12]$$

From these two facts and numerical examination it was concluded that $P_j^{ff}(\xi_s, \xi_{s_0})$ could be written in the following form,

$$P_j^{ff}(\xi_s, \xi_{s_0}) = P_j^{fu}(\xi_s, \xi_{s_0}) + P^v(\xi_s, \xi_{s_0}) + A(\xi_{s_0}), \qquad [13]$$

where $P^v(\xi_s, \xi_{s_0})$ is the variable part of $P_j^{ff}(\xi_s, \xi_{s_0})$, such that $P^v(0, \xi_{s_0}) = P^v(L, \xi_{s_0}) = 0$, and $A(\xi_{s_0}) - GL/2$ is the initial value for $n = j$ and $\xi_s = 0$. $P^v(\xi_s, \xi_{s_0})$ reads as (see Fig. 12)

$$P^v(\xi_s, \xi_{s_0}) = \tilde{P}(\xi_s + \xi_{s_0}) - \tilde{P}(\xi_{s_0}) \quad \text{for } \xi_s + \xi_{s_0} \le L \qquad [14]$$

and

$$P^v(\xi_s, \xi_{s_0}) = \tilde{P}(\xi_s + \xi_{s_0} - L) - \tilde{P}(\xi_{s_0}) \quad \text{for } \xi_s + \xi_{s_0} \ge L.$$

From now on functions with upper $\sim$ will correspond to the reference cell. It can be concluded that

$$\tilde{P}(\xi_{s_{02}}) - \tilde{P}(\xi_{s_{01}}) = A(\xi_{s_{02}}) - A(\xi_{s_{01}}). \qquad [15]$$

The intrinsic phase-averaged pressure in transition cells, $P^{ft}(\xi_s, \xi_{s_0})$, can be written similarly as

$$P^{ft}(\xi_s, \xi_{s_0}) = m \cdot P^v(\xi_s, \xi_{s_0}) - G \cdot \xi_s/2 + g(\xi_s, \xi_{s_0}), \qquad [16]$$

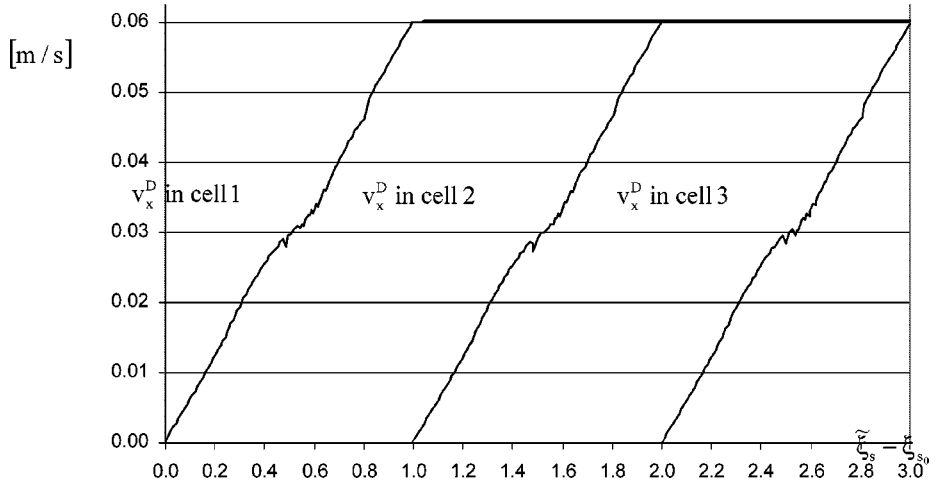

FIG. 10. Phase-averaged velocity calculated in each uniform cell separately.

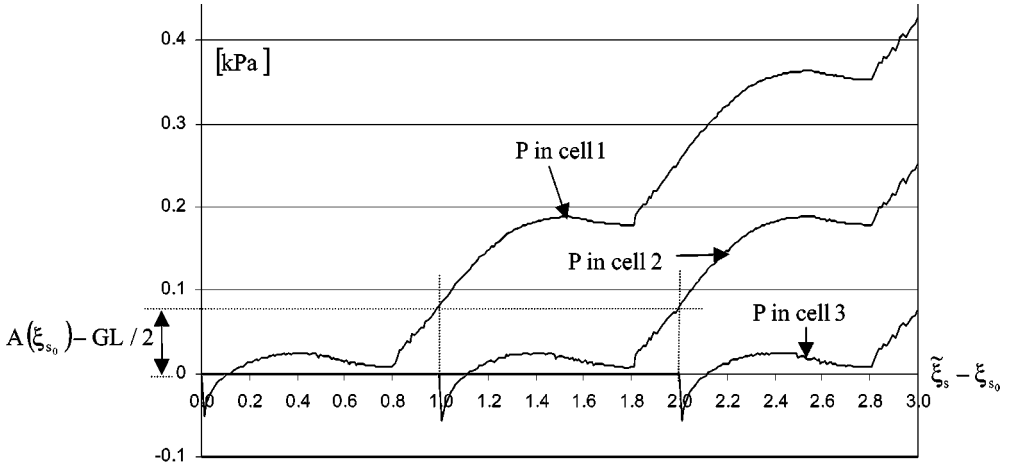

FIG. 11. Intrinsic phase averaged pressures calculated in each uniform cell separately.

where m is a coefficient and $g(\xi_s, \xi_{s_0})$ is a function, which adjust the initial and the final value. It will be seen later on that it is not necessary to determine exactly either the value of m or the exact functional dependence of $P^v(\xi_s, \xi_{s_0})$. Function $g(\xi_s, \xi_{s_0})$ must basically fulfill two conditions: (I) at $\xi_s = 0$ it reflects mainly the influence of the capillary pressure on the initial interstitial phase-averaged value and this influence rapidly diminishes with increasing ξ_s; (II) on the other hand, close to $\xi_s = L$, local fields are approaching the periodic stage, capillary pressure influence is going to be completely removed, and its influence will shift to the next transition cell. The value of function g close to $\xi_s = L$ can thus be estimated from the condition that the macroscopic pressure gradient must reach value G, which will be used later on. From continuity,

$$P^{ft}(L, \xi_{s_0}) = -GL/2 + g(L, \xi_{s_0}) = A(\xi_{s_0}) - GL/2. \quad [17]$$

Then condition (I) yield

$$P^{ft}(0, \xi_{s_0}) = g(0, \xi_{s_0}) = \frac{A(\xi_{s_0}) + P_c(0, \xi_{s_0})}{2} = \frac{g(L, \xi_{s_0}) + P_c(0, \xi_{s_0})}{2}. \quad [18]$$

Due to conditions (I) and (II) function g can be assumed in the following form,

$$g(\xi_s, \xi_{s_0}) = g(0, \xi_{s_0}) \cdot f_1(\xi_s) + g(L, \xi_{s_0}) \cdot f_2(\xi_s) = \frac{g(L, \xi_{s_0}) + P_c(0, \xi_{s_0})}{2} f_1(\xi_s) + g(L, \xi_{s_0}) \cdot f_2(\xi_s), \quad [19]$$

where functions $f_1(\xi_s)$ and $f_2(\xi_s)$ express the respective importance of these statements.

Capillary pressure can be determined analytically as a function of the resin front-fiber contact point location. For our purposes, we will need the total horizontal capillary force distributed uniformly along the vertical distance η_s (see Fig. 8). At this point we will need numerical results of the front progression, in order to relate contact point locations with ξ_s and η_s. Analytically determined values related to numerically obtained ξ_s in the reference cell are plotted in Fig. 13. Capillary pressure is uniquely related to the front position. Thus,

$$P_c(\xi_s, \xi_{s_0}) = \tilde{P}_c(\xi_s + \xi_{s_0}) \quad \text{for } \xi_s + \xi_{s_0} \le L \quad [20]$$

and

$$P_c(\xi_s, \xi_{s_0}) = \tilde{P}_c(\xi_s + \xi_{s_0} - L) \quad \text{for } \xi_s + \xi_{s_0} \ge L.$$

Macroscopic pressure gradient can be expressed as (Fig. 9)

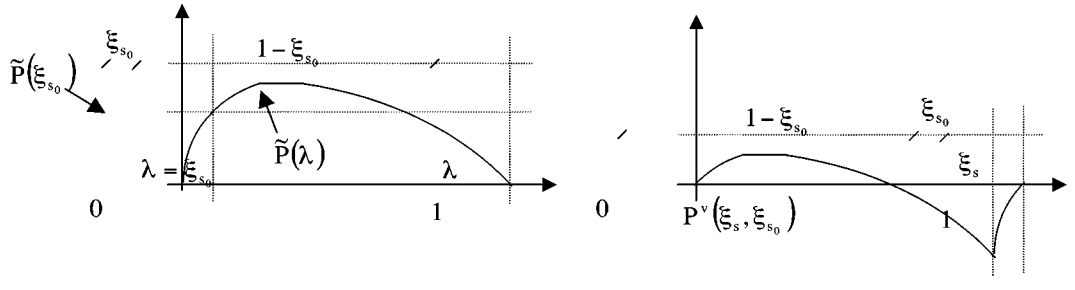

FIG. 12. Functional dependence of $P^v(\xi_s, \xi_{s_0})$.

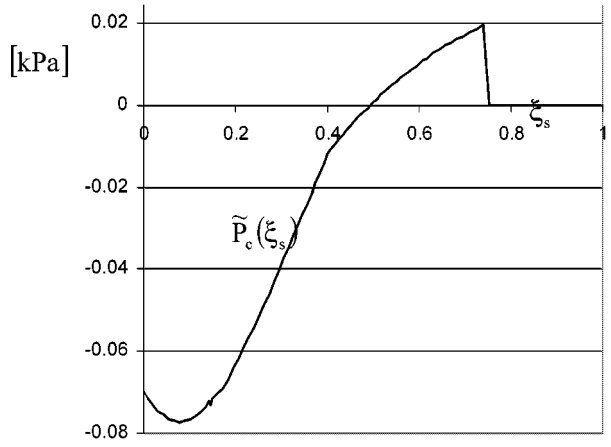

FIG. 13. Capillary pressure dependence.

$$\bar{G}(\xi_s, \xi_{s_0}) = -2\big(P^{ft}(\xi_s, \xi_{s_0}) - P_c(\xi_s, \xi_{s_0})\big)/\xi_s. \quad [21]$$

Its average over ξ_{s_0} must be performed. Since denominator of Eq. [21] is independent of ξ_{s_0}, the average of the numerator is straightforward. The phase-averaged velocity can be expressed as

$$v_x^D(\xi_s, \xi_{s_0}) = \tilde{v}_x^D(\xi_s + \xi_{s_0}) - \tilde{v}_x^D(\xi_{s_0})_{\xi_s} \quad \text{for } \xi_s + \xi_{s_0} \le L \quad [22]$$

and

$$v_x^D(\xi_s, \xi_{s_0}) = \tilde{v}_x^D(\xi_s + \xi_{s_0} - L) + \tilde{v}_x^D(L) - \tilde{v}_x^D(\xi_{s_0})_f \quad \text{for } \xi_s + \xi_{s_0} \ge L,$$

where $\tilde{v}_x^D(L) = v_{x,p}^D$ is the periodic value from the principal assumption. Values $\tilde{v}_x^D(\xi_{s_0})_{\xi_s}$ and $\tilde{v}_x^D(\xi_{s_0})_f$ are generally different; for both, velocities are integrated over the same area, but in the first case the reference cell is in the transition stage while in the second case it has achieved the saturated state. Continuity must be preserved; thus both values coincide when $\xi_s + \xi_{s_0} = L$. One can integrate the local velocity over an area including one filled reference cell and a reference transition cell in two ways. Either by selecting the reference cell as the uniform cell or by selecting the other cell as the uniform cell such that $\xi_s + \xi_{s_0} < L$. Taking into account the principal assumption, it results in $\tilde{v}_x^D(\xi_{s_0})_{\xi_s} = \tilde{v}_x^D(\xi_{s_0})_f$. Therefore local velocity distribution does not vary during filling. This does not mean that $v_x^D(\xi_s, \xi_{s_0})$ is linear with respect to ξ_s for arbitrary ξ_{s_0}, but (as will be shown below) linearity is fulfilled for the averaged value $\langle v_x^D(\xi_s, \xi_{s_0})\rangle_{\xi_{s_0}}$.

Simple analytical derivation reveals that (for any $P^v(\xi_s, \xi_{s_0})$ fulfilling (14))

$$\big\langle P_c(\xi_s, \xi_{s_0})\big\rangle_{\xi_{s_0}} = \langle \tilde{P}_c(\xi_s)\rangle_{\xi_s} = A_{P_c,\xi_s}/L = A_{P_c,\varepsilon_s};$$
$$\big\langle P^v(\xi_s, \xi_{s_0})\big\rangle_{\xi_{s_0}} = 0 \quad [23]$$

and

$$\big\langle v_x^D(\xi_s, \xi_{s_0})\big\rangle_{\xi_{s_0}} = \tilde{v}_x^D(L)\cdot \xi_s/L = v_{x,p}^D \cdot \xi_s/L = v_{x,p}^D \cdot \varepsilon_s,$$

where A_{P_c,ε_s} is the mean value of the capillary pressure related to front progression and $\varepsilon_s = \xi_s/L$ is the dimensionless counterpart of ξ_s.

Using Eqs. [16], [19], and [23], it can be shown that

$$\big\langle P^{ft}(\xi_s, \xi_{s_0}) - P_c(\xi_s, \xi_{s_0})\big\rangle_{\xi_{s_0}} = -G\cdot\xi_s/2 - A_{P_c,\varepsilon_s} + \frac{\big\langle g(L, \xi_{s_0})\big\rangle_{\xi_{s_0}} + A_{P_c}, \varepsilon_s}{2} \cdot f_1(\xi_s) + \big\langle g(L, \xi_{s_0})\big\rangle_{\xi_{s_0}} \cdot f_2(\xi_s). \quad [24]$$

Still unknown term $\langle g(L, \xi_{s_0})\rangle_{\xi_{s_0}}$ can be determined from the condition (II) ensuring for $\xi_s = L$ the result in Eq. [24] equals $-GL/2$. Since $f_1(L) = 0$ and $f_2(L) = 1$, it holds $\langle g(1, \xi_{s_0})\rangle_{\xi_{s_0}} = A_{P_c,\varepsilon_s}$. Thus,

$$\big\langle \bar{G}(\xi_s, \xi_{s_0})\big\rangle_{\xi_{s_0}} = G + 2A_{P_c,\varepsilon_s}\frac{1 - f_1(\xi_s) - f_2(\xi_s)}{\xi_s}. \quad [25]$$

Now functions $f_1(\xi_s)$ and $f_2(\xi_s)$ appear in sum, and they can be estimated simultaneously. One of the possibilities is

$$f_1(\xi_s) + f_2(\xi_s) = (2\xi_s/L - 1)^q, \quad [26]$$

where q is even. When $q = 0$, there is no non-uniformity and saturated gradient G is reached in the full range, i.e., filling is uniform. The higher the value of q, the sharper the implementation of conditions (I) and (II). Adopting $v_{x,p}^D = -(K_{xx}/\mu)G$ one can finally express the relative permeability from Eq. [3b] as

$$k_{xx} = \frac{G\cdot\xi_s/L}{G + \frac{2A_{P_c,\varepsilon_s}}{\xi_s}(1 - (2\xi_s/L - 1)^q)} = \frac{\hat{G}\cdot\varepsilon_s}{\hat{G} + \frac{2A_{P_c,\varepsilon_s}}{\varepsilon_s}(1 - (2\varepsilon_s - 1)^q)}, \quad [27]$$

where $\hat{G} = GL$.

Relative permeability in our example as function of ξ_s is shown in Fig. 14 for $q = 2$ and $q = 8$. It is seen that the difference between these two curves is not crucial. The main information from the final result is the maximum distance of $k_{xx}(\xi_s)$ from the linear function (also included in Fig. 14), which is dictated by A_{P_c,ε_s} depending on front progression. As an intermediate result, macroscopic capillary pressure $\langle P_c(\xi_s, \xi_{s_0})\rangle_{\xi_{s_0}} = A_{P_c,\varepsilon_s}$ was obtained independent of ξ_s.

Relative permeability should have tensorial character in the same way as absolute permeability **K**. Therefore in Eq. [3b] it should not appear as a scalar parameter, but different components of **K** should be multiplied by corresponding relative permeability components. It would be more appropriate to use in Eq. [3b] effective permeability tensor. For the sake of completeness,

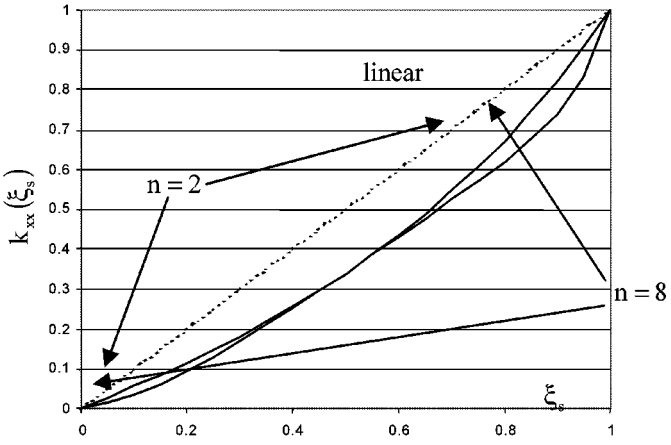

FIG. 14. Relative permeability as a function of ξ_s for $n = 2$ and 8.

our geometry has three principal directions; thus, $k_{xy} = k_{yz} = k_{xz} = 0$, $k_{yy} = k_{xx}$ and k_{zz} would have to be determined differently.

Now we can summarize the methodology and make some generalizations. From the previous discussion and derivations, it is clear that for the relative permeability determination it is sufficient to calculate analytically the local horizontal capillary force as a function of the resin front-fiber contact points. Then it is necessary to determine front progression in at least one uniform cell, distribute uniformly the capillary force along η_s, and express it as a function of ξ_s. Next it is possible to calculate A_{P_c,ε_s} as the mean value of the previous distribution, determine saturated gradient G, and use Eq. [27] with a selected non-zero and even value of q. The methodology presented here ensures that the final curve will always have values below the linear function as soon as A_{P_c,ε_s} is negative and that the boundary values will be 0 and 1. Macroscopic capillary pressure was determined as A_{P_c,ε_s}.

The same geometry was retained but other parameters were changed to test the universality of the methodology. Below we state some of our conclusions.

(a) For this case study, with the same capillary number but different surface tension γ it was concluded that front progression was the same, although A_{P_c,ε_s} is proportional to γ. In the same way for the modified G, consequently the relative permeability curve is exactly the same.

(b) For this case, the contact angle θ was varied with the same capillary number and the same value of surface tension γ. It was concluded that front progression was almost the same (in studied cases θ has small influence on bulk front progression), although A_{P_c,ε_s} is strongly influenced by θ.

(c) The case with the same surface tension γ but different capillary numbers revealed that local capillary pressure will be the same as a function of the resin front-fiber constant points. Front progression will be different. For larger capillary number than the original value contact point dependence of ξ_s and η_s will be different and A_{P_c,ε_s} will be higher. However, this change is not as large as the change in G and therefore the relative permeability curve is less curved than the original.

(d) With dimensional change in the cell where all resin parameters and capillary number are the same it was concluded that the relative permeability curve did not change.

7. CONCLUSIONS

In this paper, free boundary program and methodology for determination of relative permeability and macroscopic capillary pressure were presented. Free boundary program permits one to study resin progression at the microlevel and in this way define, for example, the range for the capillary number for a particular geometry, which will ensure air displacement by the primary mechanism.

Methodology to determine relative permeability and macroscopic capillary pressure was presented with the help of a simple example. It was concluded that surface tension as well as viscous forces influence relative permeability. More work must be done to study cases where more cells will be in transition stage simultaneously and cases with dual porosity geometry.

REFERENCES

1. Advani, S. G., Bruschke, M. V., and Parnas, R. S., *in* "Flow and Rheology in Polymeric Composites Manufacturing" (S. G. Advani. Ed.), p. 465. Elsevier, Amsterdam, 1994.
2. Bruschke, M. V., and Advani, S. G., *Polym. Compos.* **11,** 398 (1990).
3. Bruschke, M. V., and Advani, S. G., *SAMPE Q.* **22,** 2 (1991).
4. Bruschke, M. V., and Advani, S. G., A numerical approach to model non-isothermal, viscous flow with free surfaces through fibrous media, *Int. J. Numer. Methods Fluids* **19,** 575 (1994).
5. Lee, L. J., Young, W. B., and Lin, R. J., Mold filling and cure modeling of RTM and SRIM processes, *Compos. Struct.* **27,** 109 (1994).
6. Liu, B., Bickerton, S., and Advani, S. G., Modeling and simulation of resin transfer molding (RTM)-Gate control, venting, and dry spot prediction, *Composites A* **27A,** 135 (1996).
7. Gauvin, R., Trochu, F., Lemenn, Y., and Diallo, L., Permeability measurement and flow simulation through fiber reinforcement, *Polym. Compos.* **17,** 34 (1996).
8. Scheidegger, A. E., "The Physics of Flow through Porous Media." Macmillan, New York, 1957.
9. Bear, J., "Dynamics of Fluids in Porous Media." Elsevier, New York, 1972.
10. Kaviany, M., "Principles of Heat Transfer in Porous Media," 2nd ed. Springer-Verlag, New York, 1995.
11. Lundstrom, T. S., Bubble transport through constricted capillary tubes with application to resin transfer molding, *Polym. Compos.* **17,** 770 (1996).
12. Lundstrom, T. S., Void collapse in resin transfer molding, *Composites A* **28A,** 201 (1997).
13. Gebart, B. R., *J. Compos. Mater.* **26,** 1100 (1992).
14. Bruschke, M. V., and Advani, S. G., Flow of generalized Newtonian fluids across a periodic array of cylinders, *J. Rheol.* **37,** 479 (1993).
15. van der Westhuizen, J., and du Plessis, J. P., An attempt to quantify fibre bed permeability utilizing the phase average Navier-Stokes equation, *Composites A* **27A,** 263 (1996).
16. Simacek, P., and Advani, S. G., Permeability model for a woven fabric, *Polym. Compos.* **17,** 887 (1996).

17. Parnas, R. S., and Salem, A. J., A comparison of the unidirectional and radial in-plane flow of fluids through woven composite reinforcements, *Polym. Compos.* **14,** 383 (1993).
18. Wang, T. G., Wu, C., and Lee, L. J., In-plane permeability measurement and analysis in liquid composite molding, *Polym. Compos.* **15,** 278 (1994).
19. Wu, C., Wang, T. G., and Lee, L. J., Trans-plane fluid permeability measurement and its application in liquid composite molding, *Polym. Compos.* **15,** 289 (1994).
20. Parnas, R. S., Salem, A. J., Sadiq, T. A. K., Wang, H. P., and Advani, S. G., The interaction between micro- and macroscopic flow in RTM preforms, *Compos. Struct.* **27,** 93 (1994).
21. Parnas, R. S., Luce, T., Advani, S. G., and Howard, G., Permeability characterization, Part 1: A proposed standard reference material, *Polym. Compos.* **16,** 430 (1995).
22. Carter, E. J., Fell, A. W., Griffin, P. R., and Summerscales, J., Data validation procedure for the automated determination of the two-dimensional permeability tensor of a fabric reinforcement, *Composites A* **27A,** 255 (1996).
23. Mogavero, J., and Advani, S. G., Experimental investigation of flow through multi-layered preforms, *Polym. Compos.* **18,** 649 (1997).
24. Bickerton, S., and Advani, S. G., *Compos. Sci. Technol.* **57,** 23 (1997).
25. Bickerton, S., Advani, S. G., Mohan, R. V., and Shires, D. R., Experimental analysis and numerical modeling of flow channel effects in resin transfer molding, *Polym. Compos.* **20,** 12 (1999).
26. Ballata, B., Walsh, S., and Advani, S. G., Measurement of the transverse permeability of fiber preforms, *J. Reinf. Plast. Compos.* **18,** 1450 (1999).
27. Sanchez-Palencia, E., *in* "Non-Homogeneous Media and Vibration Theory" (J. Ehlers, R. Kippenhahn, and J. Zittartz, Eds.), p. 129. "Lecture Notes in Physics," Vol. 127. Springer-Verlag, Berlin, 1980.
28. Chang, W., Ph.D. dissertation, Univ. of Michigan, 1993.
29. Calado, V. M. A., and Advani, S. G., Effective permeability of multilayer preforms in resin transfer molding, *Compos. Sci. Technol.* **56,** 519 (1996).
30. Ranganathan, S., Phelan, F. R., and Advani, S. G., A generalized model for the transverse fluid permeability in unidirectional fibrous media, *Polym. Compos.* **17,** 222 (1996).
31. Dimitrovova, Z., and Faria, L., Finite element modeling of the resin transfer molding process based on homogenization techniques, *Comput. Struct.* **76,** 379 (2000).
32. Darcy, H., "Les Fontaines Publiques de la Ville de Dijon," Dalmont, Paris, 1856.
33. Sanchez-Palencia, E., On the asymptotics of the fluid flow past an array of fixed obstacles, *Int. J. Eng. Sci.* **20,** 1291 (1982).
34. Ene, H. I., and Polisevski, D., "*Thermal Flow in Porous Media.*" Reidel, Dordrecht, 1987.
35. Whitaker, S., *Transp. Porous Media* **1,** 3 (1986).
36. Dave, R., A unified approach to modeling resin during composite processing, *J. Compos. Mater.* **24,** 22 (1990).
37. Muskat, M., "The Flow of Homogeneous Fluids through Porous Media." McGraw-Hill, New York, 1937.
38. Papathanasiou, T. D., A structure oriented micromechanical model for viscous flow through square arrays of fibre clusters, *Compos. Sci. Technol.* **56,** 1055 (1996).
39. Dimitrovova, Z., and Faria, L., Proceedings of the 5th International Conference on Flow Processes in Composite Materials, July, Plymouth, UK, p. 125, 1999.
40. Phelan, F. R., and Wise, G., Analysis of transverse flow in aligned fibrous porous media, *Composites A* **27A,** 25 (1996).
41. Spaid, M. A. A., and Phelan, F. R., Lattice Boltzman method for modeling microscale flow in fibrous porous media, *Phys. Fluids* **9,** 2468 (1997).
42. Antonelli, D., and Farina, A., Resin transfer moulding: mathematical modelling and numerical simulations, *Composites A* **30,** 1367 (1999).
43. "Abaqus/Standard Theory Manual," Version 5.6. Hibbitt, Karlsson and Sorensen, 1998.
44. White, F. M., "Fluid Mechanics," 3rd ed. McGraw-Hill, New York, 1994.
45. Adamson, A. W., "Physical Chemistry of Surfaces," 5th ed. Wiley, New York, 1982.
46. ISL (Intelligent Systems Lab), http://islnotes.cps.msu.edu/trp/rtm/inj_wet.html, Tutorial on polymer composite molding, Michigan State Univ., 1997.
47. Hocking, L. M., *J. Fluid Mech.* **79,** 209 (1977).
48. Concus, P., and Finn, R., *in* "Low-Gravity Fluid Dynamics and Transport Phenomena" (J. N. Koster and R. L. Sani, Eds.), p. 183, "Progress in Astronautics and Aeronautics," Vol. 130. American Institute of Aeronautics and Astronautics, 1990.
49. Keller, A. A., Ph.D. dissertation, Stanford University, Stanford, CA, 1996.
50. Saez, A. E., Carbonell, R. G., and Levec, J., The hydrodynamics of trickling flow in packed beds, Part I: Conduit models, *AIChE J.* **32,** 353 (1986).
51. Han, K., Ph.D. dissertation, Ohio State Univ., 1994.
52. Kim, J., Ph.D. dissertation, Princeton Univ., Princeton, NJ, 1987.
53. Ahn, K. J., Seferis, J. C., and Berg, J. C., Simultaneous measurements of permeability and capillary pressure of thermosetting matrices in woven fabric reinforcements, *Polym. Compos.* **12,** 146 (1991).